Physica E 44 (2011) 525–529

Contents lists available at SciVerse ScienceDirect

Physica E

journal homepage: www.elsevier.com/locate/physe

Hyperelastic axial buckling of single wall carbon nanotubes

E.I. Saavedra Flores [a], S. Adhikari [a,*], M.I. Friswell [a], F. Scarpa [b]

[a] College of Engineering, Swansea University, Singleton Park, Swansea, SA2 8PP, United Kingdom
[b] Department of Aerospace Engineering, University of Bristol, Queens Building, University Walk, BS8 1TR Bristol, United Kingdom

ARTICLE INFO

Article history:
Received 3 August 2011
Accepted 7 October 2011
Available online 18 October 2011

ABSTRACT

This paper proposes a hyperelastic finite element-based lattice approach for the description of buckling behaviour in single wall carbon nanotubes (SWCNTs). A one-term incompressible Ogden-type hyperelastic model is adopted to describe the equivalent mechanical response of C–C bonds in SWCNTs under axial compression. The material constants of the model are chosen by matching the linearised response with the elastic constants adopted in the AMBER force field and by establishing equivalence between the Ogden strain energy and the variation of the interatomic strain energy obtained from molecular mechanics simulations. Numerical experiments are carried out and the results are compared to atomistic simulations, demonstrating the predictive capabilities of the present model in capturing initial buckling strain, deformation mechanisms and post-buckling behaviour under very large compressive deformations.

© 2011 Elsevier B.V. All rights reserved.

1. Introduction

Over the last few years, the investigation of carbon nanotubes by means of computational simulations has brought substantial progress, particularly in relation to the understanding of their mechanical behaviour [1–3]. In the context of numerical models, two main categories can be found extensively in the current literature. The first category corresponds to the atomistic approach [1,3–6], in which classical molecular dynamics and tight-binding molecular dynamics constitute the most popular techniques. Although these strategies have been demonstrated to be successful in capturing complex deformation mechanisms in atomistic systems, they suffer from the drawback of excessive computing costs and therefore, their use has been limited to the analysis of small to moderate size problems. The second category is represented by finite elements simulations [2,7–11]. Particularly in this category, the lattice approach [2,12] has been demonstrated to be a suitable technique for the analysis of carbon nanotubes. This approach establishes a linkage between structural and molecular mechanics at the C–C bond level, and provides a way to model the deformation of carbon nanotubes by means of conventional finite element analyses using classical beam elements. Curiously, despite the extensive work carried out in this context, a review of the current literature on the finite element-based lattice approach shows that the adoption of a hyperelastic framework to describe the atomic covalent bonds in SWCNTs at large strains continues to be largely ignored. Moreover, the little research reported in this context [13,14] has been restricted exclusively to the study of carbon nanotubes under axial tension. In Ref. [15], the authors also noticed the need of more efforts to better reproduce the bond energy terms within the range of large deformations.

In an attempt to encourage others researchers in this field to make use of such concepts our main objective in this paper is to adopt a hyperelastic framework in the constitutive modelling of C–C bonds in order to capture the main features of buckling behaviour in SWCNTs under axial compression. We anticipate here that with the use of such a hyperelastic model, the prediction of the initial buckling strain is achieved successfully. In addition, the model is able to reproduce the main mechanisms of deformation and to capture the post-buckling response under large strains.

We note that for very large compressive strains before buckling, the response provided by hyperelastic and linear elastic models may become very different. For instance, the importance of considering finite strain constitutive formulations in the calculation of minimum critical buckling loads has been noticed in Ref. [16]. The need of analyses and designs based on more general frameworks taking into account finite strains and the development of geometric instabilities has also been reported in Ref. [17].

We remark here that, in a recent publication [14], the authors adopted a similar approach to model C–C bonds in SWCNTs under tension. The results showed good predictive capabilities of the model. However, the strain energy associated with angular deformation, bending and torsion was calculated under purely

* Corresponding author. Tel.: +44 1792 602088, fax: +44 1792 295676.
E-mail address: s.adhikari@swansea.ac.uk (S. Adhikari).

1386-9477/$ - see front matter © 2011 Elsevier B.V. All rights reserved.
doi:10.1016/j.physe.2011.10.006

mechanical considerations rather than adopting an atomistic criteria. Here, this drawback is circumvented by allowing the present model to recover the AMBER force model [18] constants for stretching, angle bending and torsion in the range of infinitesimal strains. Moreover, we explore the suitability of this hyperelastic description when the radius and the length of carbon nanotubes are varied in a detailed set of numerical experiments. The paper is organised as follows. Section 2 presents the description of the equivalent mechanical response of C–C bonds in SWCNTs by means of a hyperelastic framework. The validation of the present model is given in Section 3. Finally, Section 4 summarises our conclusions.

2. Hyperelastic description

A generic finite hyperelastic model is characterised by the existence of a strain energy density function Ψ, which defines the evolution of the Kirchhoff stress tensor, $\boldsymbol{\tau}$, in terms of the current *Eulerian logarithmic strain* tensor, $\boldsymbol{\varepsilon}$. The constitutive equation for the Kirchhoff stress tensor is given by [19,20]

$$\boldsymbol{\tau} = \frac{\partial \Psi}{\partial \boldsymbol{\varepsilon}}. \tag{1}$$

The strain tensor $\boldsymbol{\varepsilon}$ can be represented as a function of the *left stretch tensor*, $\boldsymbol{V}$, by means of the expression $\boldsymbol{\varepsilon} = \ln \boldsymbol{V}$. Furthermore, if the strain energy function Ψ is assumed to be isotropic, it is possible to adopt a representation for $\boldsymbol{V}$ in terms of the principal stretches, λ_i, $i = 1 \ldots 3$. Hence, we can write the constitutive equation for the eigenvalues τ_i of the Kirchhoff stress tensor as

$$\tau_i = \frac{\partial \Psi}{\partial \ln(\lambda_i)}. \tag{2}$$

The particular choice of the strain energy density Ψ is commonly considered to be a matter of mathematical or experimental convenience. Here, due to its simplicity and predictive accuracy for large deformations in conventional materials, an Ogden hyperelastic isotropic material model [21] is chosen for the mechanical modelling of C–C bonds. A one-term incompressible version of the Ogden strain energy density function is adopted, whose expression is given by

$$\Psi = \frac{2\chi}{\alpha^2}\{(\lambda_1)^\alpha + (\lambda_2)^\alpha + (\lambda_3)^\alpha - 3\}, \tag{3}$$

where χ and α are material parameters to be determined.

2.1. Mechanical response for infinitesimal strains. Choice of the constant χ and the actual shear stiffness GA_s

In order to capture the mechanical response of C–C bonds in the range of infinitesimal strains, we proceed to match the linearised response of the present hyperelastic model with the linear elastic constants adopted in the AMBER force model.

The value of the constant χ in Eq. (3) is related to the linear elastic shear modulus G, through the condition $\chi = G$ (we refer here to Refs. [22,23]). In the limit of incompressibility, the shear modulus becomes $E/3$ in isotropic solids. Thus, we obtain the relationship:

$$\chi = \frac{E}{3}. \tag{4}$$

By establishing equivalence between the interatomic energies and their mechanical counterparts by means of the lattice representation [2], in which C–C bonds are assumed to behave as structural beam elements with circular cross-section of diameter d, and length L, it is straightforward to obtain the expression:

$$E = \frac{4K_r L}{\pi d^2}. \tag{5}$$

The length L is given by the equilibrium bond length between carbon atoms and is considered here as 0.142 nm [24]. The parameter K_r is the bond stretching constant and is assumed to be 652.2 nN nm^{-1} [25]. The C–C bond equivalent diameter adopted in this work is $d = 0.10$ nm. As shall be seen later in this section, the adoption of this value allows us to reproduce a phenomenological response similar to that found numerically in molecular simulations [15]. We also note that a value of $d = 0.1$ nm has been previously identified in graphene sheets under non-linear out-of-plane bending [24,12]. By evaluating the expressions (4) and (5) with the above data, the resultant values for the Young modulus and Ogden constant are $E = 11.8$ TPa and $\chi = 3.93$ TPa, respectively.

If we take into account the shear effects present in the deformation of C–C bond beams [24], the mechanical bending stiffness can be expressed as

$$K_\theta = \frac{EI(4+\phi)}{L(1+\phi)}, \quad \text{with } \phi = \frac{12EI}{GA_s L^2}, \tag{6}$$

where the factor GA_s is referred to as the *actual shear stiffness*. The parameter I is the second moment of area and is defined for a circular cross-section as $I = \pi d^4/64$. Furthermore, if we establish equivalence between the mechanical bending strain energy and the interatomic angle bending energy, we obtain that the bending stiffness K_θ is equivalent to the AMBER angle bending force constant, considered here as 1.3905 nN nm rad^{-2} [25]. With the above data at hand, we can obtain that the actual shear stiffness is $GA_s = 141.24$ nN.

By taking into account isotropic condition Eq. (4), the standard expression for the mechanical torsional stiffness can be expressed as

$$K_\tau = \frac{\chi J}{L}, \tag{7}$$

where J is the polar second moment of area, defined as $J = \pi d^4/32$. By replacing the values of χ, J and L into Eq. (7), we obtain $K_\tau = 0.272$ nN nm, which is in agreement with the AMBER torsional force constant reported in the literature, equal to 0.278 nN nm rad^{-2} [24].

With the choice of the above values for the material constant χ and the actual shear stiffness GA_s, we enable the present hyperelastic model to recover the AMBER bond stretching, angle bending and torsional force constants, in the infinitesimal strains regime.

2.2. Choice of the constant α

The choice of the constant α in Eq. (3) is made by investigating the influence of this parameter on the strain energy obtained in an armchair (5,5) SWCNT finite element model, with 5 nm length. We use the commercial finite element software ABAQUS [26] to carry out all our simulations. Because of the development of local instabilities during the non-linear deformation process, we adopt the *automatic stabilisation method* provided by ABAQUS in order to capture the buckling and post-buckling response.

The finite element mesh consists of 410 nodes and 605 beam elements. We select the two-noded hybrid beam element, which will be adopted in all of the subsequent analyses presented in this paper. Transverse shear strains (Timoshenko beam theory) are considered in the beam element formulation. This type of hybrid beam element is compatible with the adoption of a hyperelastic Ogden model. The Z-axis corresponds to the axial (longitudinal) direction of the tube, whereas X and Y correspond to the

transverse directions. Zero prescribed displacements are imposed on all of the degrees of freedom of the nodes located at one of the ends of the tube, at $Z=0$. On the opposite end, at $Z=5$ nm, we apply incremental compressive displacements in the axial direction until buckling occurs. The prescribed displacements on the remaining degrees of freedom at this end are set to zero. Because the covalent bond among atoms is the dominant atomic interaction, we do not consider explicitly the effects of van der Waals forces in this paper [27].

We proceed to study the influence of the constant α on the amount of strain energy when this parameter is equal to -5.0, 2.0 and 10.0. The results obtained from our finite element simulations are compared in Fig. 1 with that obtained from molecular mechanics simulations [15]. We remark that for consistency, all the results reported in Ref. [15] and presented in this paper have been obtained by means of the application of prescribed displacements rather than forces.

We observe in Fig. 1 that the variation of α has little influence on the amount of energy when small strains are considered. Furthermore, we observe that a reduction/increase of α is accompanied by an increase/reduction in the critical buckling strain. Particularly, for $\alpha=2.0$ our model shows a clear first instant of buckling at 0.082 strain, which is in good agreement with the predicted value reported in Ref. [15], equal to 0.081. In addition, for this particular choice of α we illustrate in Fig. 2 the morphological agreement between the buckling mechanism in the finite element and molecular mechanics models, demonstrating the agreement between the phenomenological response of both approaches. Consequently, $\alpha=2.0$ will be adopted in all of the following analyses.

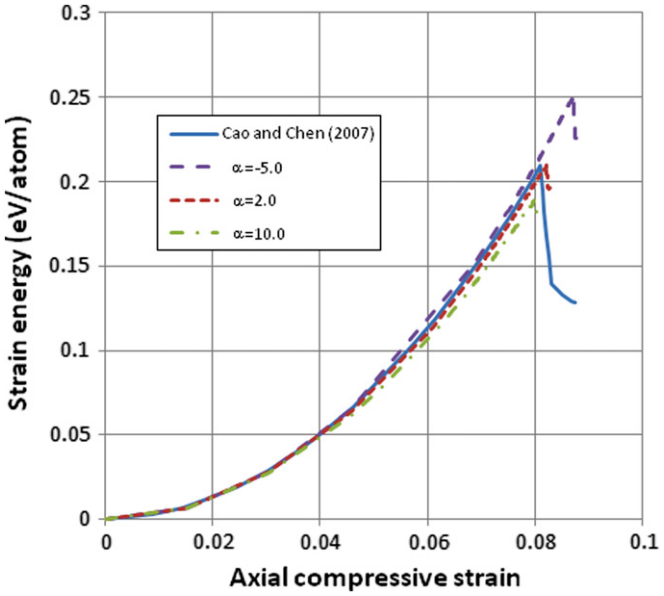

Fig. 1. Strain energy per atom for a (5,5) SWCNT with 5 nm length. Comparison between the Ogden strain energy calculated from finite element simulations considering three different values for α and the strain energy obtained from molecular mechanics simulations [15].

3. Validation of the model

Our purpose in this section is to validate the present hyperelastic model with published data. All of the considerations made in Section 2.2 in terms of modelling are applied here. Constants $\chi=3.93$ TPa and $\alpha=2.0$ are used in the model, along with a C–C bond equivalent diameter of $d=0.10$ nm and an actual shear stiffness of $GA_s=141.24$ nN. The commercial software ABAQUS [26] is used in all our computational simulations.

3.1. Compression of a zig-zag (9,0) SWCNT

In this first numerical experiment, we analyse a zig-zag (9,0) SWCNT, with 5 nm length, compressed up to the first buckling point. The corresponding finite element mesh consists of 432 nodes and 639 beam elements. The resultant strain energy per atom calculated with the present hyperelastic model is shown in Fig. 3, along with the strain energy calculated by means of molecular mechanics simulations [15] for the same geometry. We observe here a good agreement between both approaches. The evolution of the deformation energy is well predicted with nearly perfect matching up to 0.07 strain, with only a slight discrepancy in the critical buckling strains. Such critical strains are 0.082 and 0.078 for the finite element and the molecular mechanics models, respectively, revealing only a 5% difference.

3.2. Variation of the radius in carbon nanotubes

Here, we explore the suitability of the present hyperelastic description for SWCNTs within a wide range of radii, between 2 and 24 Å approximately. We compare the initial buckling strains obtained with the proposed hyperelastic model and those critical strains obtained from Refs. [28,15] (among others) in Fig. 4. Here, we can observe a good agreement between the buckling strains predicted by our numerical simulations and those calculated with molecular mechanics simulations [15], molecular dynamics models [3,5,29] and with generalized tight-binding molecular dynamics and ab initio electronic structure methods [30], which demonstrate the good predictive capabilities of the present model. For the smaller radii between 3 and 7 Å, our numerical predictions tend to fit very well to the results achieved in Ref. [15] in armchair and zig-zag carbon nanotubes. For greater radii, our critical strains show a good agreement, although slightly overestimated, with the values presented in Ref. [28] and obtained from Ref. [5]. This slight overestimation can be attributed to the fact that in Ref. [5], the authors used much longer carbon nanotubes in their simulations. Nevertheless, more information on large carbon nanotubes is needed here in order to achieve a better comparison. Table 1 also summarises the different carbon nanotubes analysed in this subsection by means of the proposed model along with their corresponding critical strains.

3.3. Variation of the length in carbon nanotubes

In this subsection we study the suitability of the proposed hyperelastic model for SWCNTs for a wide range of lengths. Here, we calculate the initial buckling strains of an armchair (10,10)

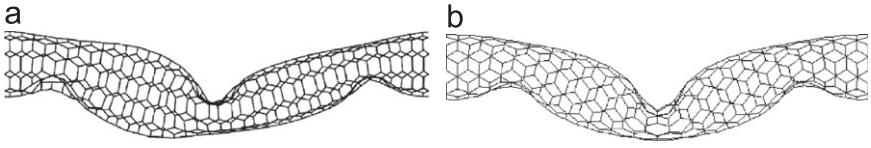

Fig. 2. Comparison of buckling mechanisms in a (5,5) SWCNT with 5.0 nm length. (a) Molecular mechanics simulation [15] and (b) present hyperelastic finite element model.

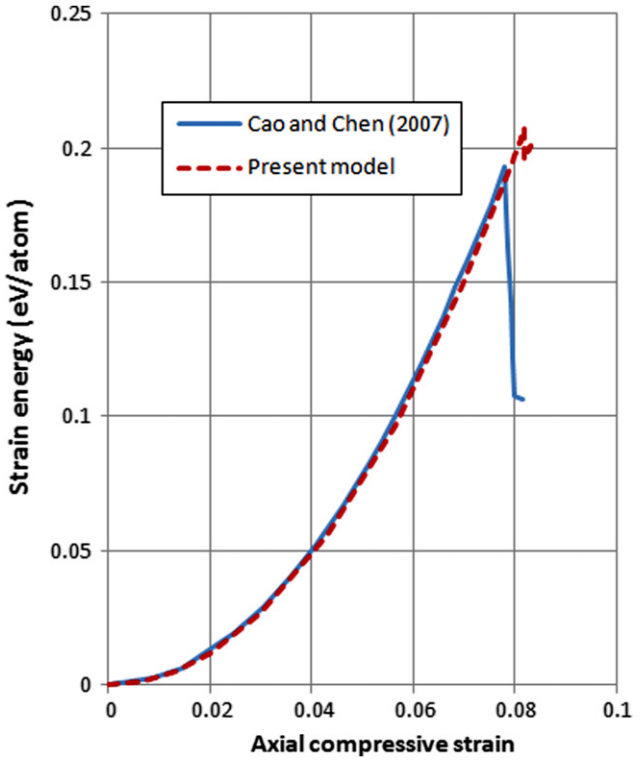

Fig. 3. Variation of the strain energy per atom during compression of a (9,0) SWCNT of 5 nm length. Comparison between the present hyperelastic finite element model and the results reported by molecular mechanics simulations [15].

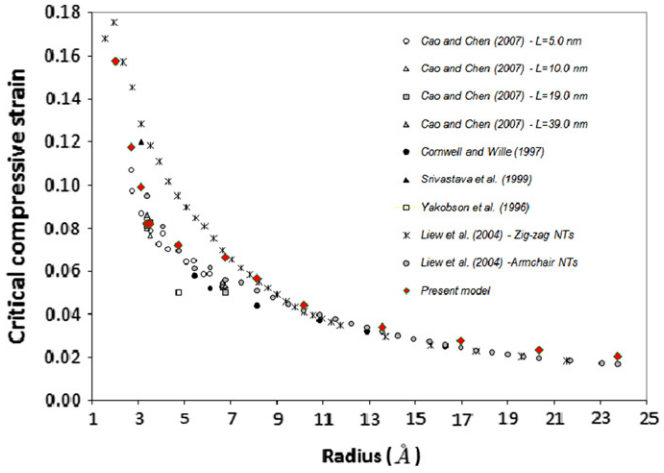

Fig. 4. Variation of the initial buckling strains according to the carbon nanotubes radius. Results obtained from the present hyperelastic model and those obtained from Refs. [28,15], among others.

SWCNT with lengths ranging between 2.5 and 14 nm, approximately. Our numerical results are presented in Fig. 5 and compared with those values obtained from molecular dynamics simulations [5]. The comparison reveals an excellent agreement between these two approaches. The difference between the critical strain calculated with finite elements and with molecular dynamics vary from 2.3% to 7.4% with an average value of 4.2%.

3.4. Post-buckling response of an armchair (7,7) SWCNT

Fig. 6 illustrates the variation of the strain energy per atom and the deformation mechanisms from our finite element simulations during the compression of a (7,7) SWCNT of 6 nm length.

Table 1
Summary of the carbon nanotubes analysed with the present hyperelastic model and shown in Fig. 4.

Chiral vector	Approx. length (nm)	Critical strain
(3,3)	4	0.158
(4,4)	5	0.118
(8,0)	4	0.099
(5,5)	5	0.082
(9,0)	5	0.082
(7,7)	6	0.072
(10,10)	5	0.067
(12,12)	6	0.057
(15,15)	8	0.044
(20,20)	8	0.034
(25,25)	10	0.028
(30,30)	10	0.023
(35,35)	10	0.021

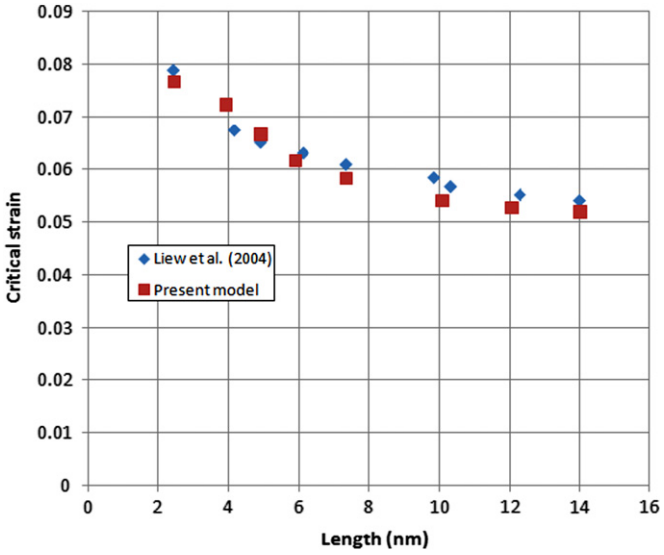

Fig. 5. Critical strains for (10,10) SWCNTs with different lengths.

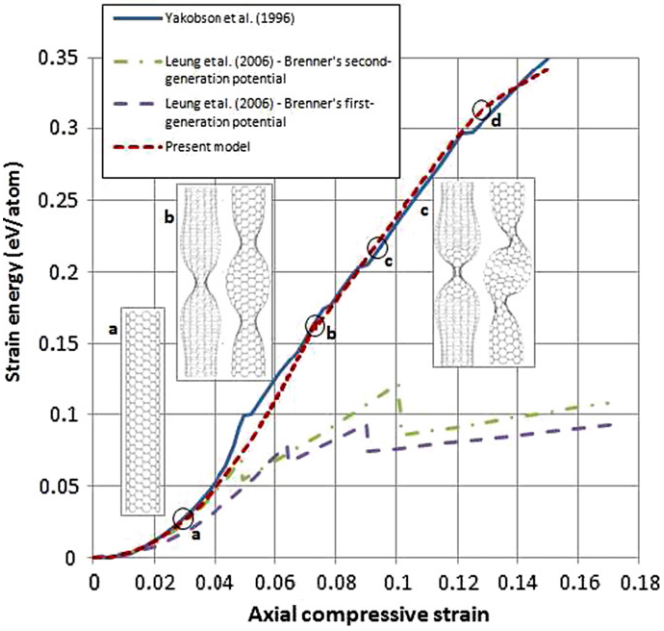

Fig. 6. Three typical configurations of the deformed (7,7) SWCNT.

Furthermore, the strain energy reported in Ref. [27], using Brenner's first [31] and second [32] generation potential, and also the strain energy calculated in Ref. [3], for the same geometry, are also presented here. The finite element mesh consists of 686 nodes and 1015 beam elements.

In a first nearly quadratic regime, the results obtained with our simulation and those obtained from Refs. [3,27], using Brenner's second generation potential, show perfect matching, up to 0.03 strain. Here, the deformation is uniform as shown in inset (a).

As the compressive deformation progresses these curves tend to diverge up to 0.05 strain in which the molecular dynamics simulation from Ref. [3] and the atomic-scale finite element model from Ref. [27] using Brenner's second generation potential reach the first instant of buckling. At this stage, Yakobson's simulation displays (although not shown here) two identical flattenings perpendicular to each other, non-symmetrically located along the tube axis. The first buckling mechanism in our simulation is found at a later stage, at 0.072 strain, coinciding closely with the second buckling strain reported by Yakobson, at 0.076. At this point, if we compare the morphological patterns in both cases we will observe that they match perfectly. In any case, our first critical strain of 0.072 and that reported by Yakobson (0.05) are depicted in Fig. 4, revealing a slight underestimation for Yakobson's result when other references are considered (see results for a radius about 4.75 Å). Inset (b) shows two orthogonal views of the first buckling deformation mechanism predicted by our numerical simulation, characterised by a three axial half-waves symmetric configuration with a still straight axis. Furthermore, we observe that despite the small difference detected at about 0.05 strain between the amount of energy reported by Yakobson and our model, at a strain about 0.07 the results predicted by both simulations tend to converge into the same amount of stored energy. In contrast, despite the fact that Leung's simulations seem to show a similar deformation mechanism (not shown here), the amount of energy reported in both cases, with Brenner's first and second generation potential, is substantially lower.

Further increase of the compressive deformation results in a new mechanism of deformation, represented by a buckling sideways in which the corresponding flattenings serve as hinges. Inset (c) plots this stage (with two perpendicular views) in our finite element simulation, revealing the preservation of only one plane of symmetry after buckling. Yakobson's simulation predicts this critical strain at 0.09. However, our numerical model varies gradually (discontinuity not visible in the curve) but during a transition which occurs at about this level of strain. In any case, we find again a morphological agreement between both methodologies. Moreover, the amount of energy calculated in these two simulations shows almost a perfect match to over 0.12 strain, where a new buckling mechanism is triggered. Yakobson reported over this level of deformation an entirely squashed asymmetric configuration. Our numerical model predicts after 0.125 strain (refer to Fig. 6, circle labelled with letter d) a morphological pattern (not shown here) similar to that shown in inset (c) but much more distorted. Beyond this point, a gradual transition in the slope of our curve is observed, revealing a slightly lower slope when compared to Yakobson's results. Here, the van der Waals interactions and other different atomic energy terms are crucial in order to describe accurately the mechanical response of carbon nanotubes for even further levels of deformations.

4. Conclusions

The buckling behaviour of single wall carbon nanotubes (SWCNTs) has been investigated by means of a finite element-based lattice approach. A one-term incompressible Ogden-type hyperelastic model has been chosen to describe the equivalent mechanical response of C–C bonds in SWCNTs under axial compression. Finite element simulations have been carried out on SWCNT models and the results have been compared to published data, demonstrating the predictive capability of the present hyperelastic model. The proposed description has been able to capture key features in the buckling behaviour of carbon nanotubes such as initial buckling strain, deformation mechanisms and post-buckling behaviour under large deformations. In addition, the suitability of this hyperelastic description has also been assessed successfully for a wide range of carbon nanotubes geometries, revealing the potential applications of our approach on the study of fullerenes.

Acknowledgements

The authors acknowledge funding from the European Research Council through Grant No. 247045 entitled "Optimisation of Multiscale Structures with Applications to Morphing Aircraft".

References

[1] S. Iijima, C. Brabec, A. Maiti, J. Bernholc, Journal of Chemical Physics 104 (1996) 2089.
[2] C. Li, T.W. Chou, International Journal of Solids and Structures 40 (2003) 2487.
[3] B. Yakobson, C. Brabec, J. Bernholc, Physical Review Letters 76 (1996) 2511.
[4] E. Hernandez, C. Goze, P. Bernier, A. Rubio, Physical Review 80 (1998) 4502.
[5] K.M. Liew, C.H. Wong, X.Q. He, M.J. Tan, S.A. Meguid, Physical Review B 69 (2004) 115429.
[6] K. Mylvaganam, L.C. Zhang, Carbon 42 (2004) 2025.
[7] R. Batra, A. Sears, International Journal of Solids and Structures 44 (2007) 7577.
[8] X. Chen, C. Cao, Nanotechnology 17 (2006) 1004.
[9] N. Hu, K. Nunoya, D. Pan, T. Okabe, H. Fukunaga, International Journal of Solids and Structures 44 (2007) 6535.
[10] C. Li, T.W. Chou, Mechanics of Materials 36 (2004) 1047.
[11] K.I. Tserpes, P. Papanikos, Composites Part B: Engineering 36 (2005) 468.
[12] F. Scarpa, S. Adhikari, C. Remillat, Nanotechnology 21 (2010) 125702.
[13] X. Ling, S. Atluri, Computer Modelling in Engineering and Science 21 (2007) 81.
[14] E.I. Saavedra Flores, S. Adhikari, M.I. Friswell, F. Scarpa, Computational Materials Science 50 (2011) 1083.
[15] G. Cao, X. Chen, International Journal of Solids and Structures 44 (2007) 5447.
[16] M.M. Attard, G.W. Hunt, International Journal of Solids and Structures 45 (2008) 4322.
[17] S. Rahmatalla, C.C. Swan, AIAA Journal 41 (2003) 1180.
[18] W.D. Cornell, P. Cieplak, C.I. Bayly, I.R. Gould, K.M. Merz, D.M. Ferguson, D.C. Spellmeywer, T. Fox, J.W. Caldwell, P.A. Kollman, Journal of the American Chemical Society 117 (1995) 5179.
[19] E.A. de Souza Neto, D. Perić, D.R.J. Owen, Computational Methods for Plasticity: Theory and Applications, Chichester, Wiley, 2008.
[20] J. Lemaitre, J.L. Chaboche, Mechanics of Solid Materials, Cambridge University Press, Cambridge, 1990.
[21] R.W. Ogden, Non-linear elastic deformations, Ellis Horwood, Chichester, 1984.
[22] A. Selvadurai, Journal of the Mechanics and Physics of Solids 54 (2006) 1093.
[23] R. Hauptmann, K. Schweizerhof, S. Doll, International Journal for Numerical Methods in Engineering 49 (2000) 1121.
[24] F. Scarpa, S. Adhikari, Journal of Physics D: Applied Physics 41 (2008) 085306.
[25] N. Hu, H. Fukunaga, C. Lu, M. Kameyama, B. Yan, Proceeding of the Royal Society A: Mathematical, Physical & Engineering Sciences 461 (2005) 1685.
[26] ABAQUS, Analysis User's Manual. Version 6.4, Hibbitt, Karlsson and Sorensen, Inc., Rhode-Island. USA, 2003.
[27] A. Leung, X. Guo, X. He, H. Jiang, Y. Huang, Journal of Applied Physics 99 (2006) 124308.
[28] N. Silvestre, International Journal of Solids and Structures 45 (2008) 4902.
[29] C.F. Corwell, L.T. Wille, Solid State Communications 101 (1997) 555.
[30] D. Srivastava, M. Menon, K. Cho, Physical Review Letters 83 (1999) 2973.
[31] D. Brenner, Physical Review B 42 (1990) 9458.
[32] D. Brenner, O. Shenderova, J. Harrison, S. Stuart, B. Ni, S. Sinnott, Journal of Physics: Condensed Matter 14 (2002) 783.